Imprinting Vortices in a Bose-Einstein Condensate using Topological Phases

A. E. Leanhardt, A. Görlitz,* A. P. Chikkatur, D. Kielpinski, Y. Shin, D. E. Pritchard, and W. Ketterle†

Department of Physics, MIT-Harvard Center for Ultracold Atoms, and Research Laboratory of Electronics, Massachusetts Institute of Technology, Cambridge, Massachusetts, 02139

(Received 16 June 2002; published 22 October 2002)

Vortices were imprinted in a Bose-Einstein condensate using topological phases. Sodium condensates held in a Ioffe-Pritchard magnetic trap were transformed from a nonrotating state to one with quantized circulation by adiabatically inverting the magnetic bias field along the trap axis. Using surface wave spectroscopy, the axial angular momentum per particle of the vortex states was found to be consistent with $2\hbar$ or $4\hbar$, depending on the hyperfine state of the condensate.

DOI: 10.1103/PhysRevLett.89.190403 PACS numbers: 03.75.Fi, 03.65.Vf, 67.40.Db, 67.40.Vs

As superfluids, Bose-Einstein condensates support rotational flow only through quantized vortices. The atomic velocity field is proportional to the gradient of the phase associated with the macroscopic wave function. This phase winds through an integer multiple of 2π radians around a vortex line. Such a phase winding can be imprinted onto the condensate wave function either dynamically or topologically. Dynamically, the phase of the condensate evolves according to the time integral of its energy, which can be tailored locally with a spatially varying external potential. Topologically, the phase of the condensate advances through adiabatic variations in the parameters of the Hamiltonian governing the system. This phase, which is solely a function of the path traversed by the system in the parameter space of the Hamiltonian, is known as Berry's phase [1].

In this Letter, we implement the proposal of Refs. [2–5] and demonstrate the use of topological phases to imprint vortices in a gaseous Bose-Einstein condensate. Previously, vortices have been generated in two-component condensates using a dynamical phase-imprinting technique [6] and in single-component condensates by rotating the cloud with an anisotropic potential [7–10], by slicing through the cloud with a perturbation above the critical velocity of the condensate [8,11], and through the decay of solitons [12,13]. In this work, ^{23}Na condensates were prepared in either the lower, $|F, m_F\rangle = |1, -1\rangle$, or upper, $|2, +2\rangle$, hyperfine state and confined in a Ioffe-Pritchard magnetic trap. Vortices were created by adiabatically inverting the magnetic bias field along the trap axis and could be removed by returning the bias field to its original direction. Using surface wave spectroscopy [14–16], we measured the axial angular momentum per particle of the $|1, -1\rangle$ and $|2, +2\rangle$ vortex states to be consistent with $-2m_F\hbar$ as predicted [2–5].

A Ioffe-Pritchard magnetic trap consists of an axial bias field (with curvature) and a two-dimensional quadrupole field in the orthogonal plane [17,18]:

$$\vec{B}(x, y, z) = B_z\hat{z} + B'(x\hat{x} - y\hat{y}), \quad (1)$$

where B' is the radial magnetic field gradient and quadratic terms have been neglected. For a condensate of radial extent R, inverting B_z from $B_z \gg B'R > 0$ to $B_z \ll -B'R < 0$ rotates the atomic angular momentum, $\vec{F}$, by π radians. While all atomic angular momenta rotate through the same angle, a relative phase is established across the condensate because the angular momenta rotate about a unit vector $\hat{n}(\phi) = \sin\phi\hat{x} + \cos\phi\hat{y}$ that depends on the azimuthal angle, ϕ, describing the atomic position [Fig. 1(a)].

As B_z is inverted, $\vec{F}$ adiabatically follows $\vec{B}(x, y, z)$, and the condensate remains in the state $|F, m_F\rangle$ with respect to the local magnetic field. However, in a basis

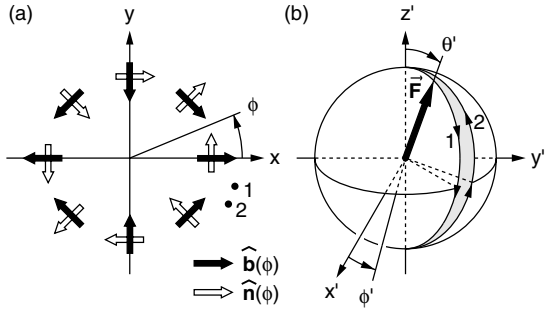

FIG. 1. Geometry of the rotating magnetic field for imprinting topological phases. (a) The unit vectors $\hat{b}(\phi)$ point in the direction of the two-dimensional quadrupole field providing the radial confinement of a Ioffe-Pritchard magnetic trap. The atomic angular momenta rotate about the unit vectors $\hat{n}(\phi)$ as the axial bias field, B_z, is ramped from positive to negative values. (b) For an atom in state $|F, m_F\rangle$, its atomic angular momentum, $\vec{F}$, traverses a path on a sphere of radius $|m_F|\hbar$ as it adiabatically follows its local magnetic field. The primed coordinate system is centered on the atomic position and has axes parallel to those of the unprimed coordinate system in (a). For an atomic position described by the azimuthal angle ϕ, $\vec{F}$ rotates in a half-plane defined by $\phi' = -\phi$ for $m_F > 0$ and $\phi' = -\phi + \pi$ for $m_F < 0$ as B_z is inverted. After inverting B_z, the relative topological phase acquired between atoms located at positions 1 and 2 in (a) is proportional to the solid angle subtended by the shaded surface, bounded by the contour marked with arrowheads (see text).

fixed in the lab frame, the condensate makes the transition $|F, m_z = +m_F\rangle \rightarrow |F, m_z = -m_F\rangle$, where m_F and m_z are the projection of $\vec{F}$ along the local magnetic field direction and z axis, respectively. Applying the quantum mechanical rotation operator gives the condensate wave function in the lab frame after inverting B_z as

$$|\psi\rangle = e^{-i(\vec{\mathcal{F}}/\hbar)\cdot\hat{\mathbf{n}}(\phi)\pi}\sqrt{\rho(\vec{r})}|F, m_z = +m_F\rangle, \quad (2)$$

$$= (-1)^{F+m_F}\sqrt{\rho(\vec{r})}e^{-i2m_F\phi}|F, m_z = -m_F\rangle, \quad (3)$$

where $\vec{\mathcal{F}}$ is the angular momentum operator such that $\vec{F} = \langle\vec{\mathcal{F}}\rangle$ and $\rho(\vec{r})$ is the number density of condensed atoms. The topological phase factor $e^{-i2m_F\phi}$ describes a vortex of winding number $2|m_F|$ with the sense of rotation dependent on the sign of m_F.

This result can be interpreted in terms of Berry's phase [4]. Figure 1(b) shows the orientation of $\vec{F}$ in the lab frame for $m_F > 0$. Atoms located at position $k = 1, 2$ in Fig. 1(a) have azimuthal angle ϕ_k and angular momentum $\vec{F}_k$. As B_z is inverted, $\vec{F}_k$ traces path k from top to bottom on the sphere in Fig. 1(b). The topological phase acquired by an atom in this process is solely a function of the path traversed by its angular momentum vector. Since this path depends on the azimuthal angle describing the atomic position, a relative phase is established between spatially separated atoms. The condensate wave function after inverting B_z is given by

$$|\psi\rangle = \sqrt{\rho(\vec{r})}e^{i\gamma(\phi)}|F, m_F\rangle, \quad (4)$$

where $\gamma(\phi)$ is the topological phase acquired by atoms with azimuthal angle ϕ.

For an atom in state $|F, m_F\rangle$, Berry's phase, $\gamma(C)$, acquired as its angular momentum vector traverses a closed contour, C, on the surface of the sphere in Fig. 1(b) is given by [1]

$$\gamma(C) = -m_F\Omega(C), \quad (5)$$

where $\Omega(C)$ is the solid angle subtended by a surface bounded by the contour C. Calculating the relative phase, $\gamma(\phi_1) - \gamma(\phi_2)$, with the aid of Eq. (5) requires closing the contours traced by each $\vec{F}_k$ along an identical path. For clarity, we choose to close each contour along path 2 itself, and hence $\gamma(\phi_1) - \gamma(\phi_2) = \gamma(C)$, where C is the contour formed by path 1 traversed from top to bottom and path 2 traversed from bottom to top, as indicated with arrowheads in Fig. 1(b).

A surface bounded by this contour subtends a solid angle $\Omega(C) = 2(\phi_1 - \phi_2)$, yielding a relative phase $\gamma(\phi_1) - \gamma(\phi_2) = -2m_F(\phi_1 - \phi_2)$. Thus, we set

$$\gamma(\phi) = -2m_F\phi, \quad (6)$$

up to an additive term independent of position. This yields a reinterpretation of Eq. (3) in terms of Berry's phase.

In this work, Bose-Einstein condensates containing over 10^7 ^{23}Na atoms were created in the $|1, -1\rangle$ state in a magnetic trap, captured in the focus of an optical tweezers laser beam, and transferred into an auxiliary "science" chamber as described in Ref. [19]. While optically confined by the tweezers, $|2, +2\rangle$ condensates were generated by sweeping through the $|1, -1\rangle \leftrightarrow |1, 0\rangle \leftrightarrow |1, +1\rangle$ radio-frequency transition with 100% efficiency, then sweeping through the $|1, +1\rangle \leftrightarrow |2, +2\rangle$ microwave transition with 80% efficiency [20]. In the science chamber, the condensate was loaded into a microfabricated Ioffe-Pritchard magnetic trap formed by a Z-shaped wire carrying current I and an external magnetic bias field, $B_\perp$, as detailed in Ref. [21]. Condensates were detected via axial absorption imaging whereby resonant laser light propagating along the z axis illuminated the atoms and was imaged onto a CCD camera.

Typical wire-trap parameters were $I = 1200$ mA, $B_\perp = 5.4$ G, and $B_z \approx 1$ G, resulting in a radial magnetic field gradient of $B' = 120$ G/cm. For $|1, -1\rangle$ ($|2, +2\rangle$) condensates, the axial and radial trap frequencies were $\omega_z = 2\pi \times 6.0$ Hz ($\omega_z = 2\pi \times 8.5$ Hz) and $\omega_\perp = 2\pi \times 210$ Hz ($\omega_\perp = 2\pi \times 300$ Hz), respectively. After transfer into the wire trap, condensates in the $|1, -1\rangle$ ($|2, +2\rangle$) state contained over 2×10^6 atoms (1×10^6 atoms) and had a lifetime in excess of 10 s (3 s) with an applied radio-frequency shield. This represents the first magnetic trapping of ^{23}Na condensates in the upper hyperfine level, with previous work done exclusively in optical dipole traps [20].

Along the wire-trap axis, the magnetic field is

$$\vec{B}(x = 0, y = 0, z) = (B_z + \tfrac{1}{2}B''z^2)\hat{z}, \quad (7)$$

where quadratic terms neglected in Eq. (1) have been included. The axial magnetic field curvature, B'', which arises from the geometry of the Z wire, was held constant throughout the experiment. By reversing an external axial magnetic field, we inverted B_z. Changing the sign of B_z, but not B'', resulted in a magnetic field saddle point at the center of the cloud and axial antitrapping of weak-field seeking atoms. This limited the condensate lifetime after inverting B_z to $\lesssim 50$ ms.

Vortices created by inverting B_z were observed after ballistic expansion and were identified by central density depletions due to the angular momentum barrier associated with a rotating cloud (Fig. 2). These vortices could be removed by returning B_z to its original direction.

For $|1, -1\rangle$ condensates, the best results were achieved by inverting the axial bias field linearly from $B_z = 860$ mG to -630 mG in 11 ms. For $|2, +2\rangle$ condensates, the optimum ramp time over the same range was 4 ms. The field inversion process caused an atom loss of $\approx 50\%$ due to nonadiabatic spin flips as B_z passed through zero [4,5]. The density depletions shown in Figs. 2(b), 2(c), and 2(g) were observed after inverting the axial bias field and holding the trapped condensate for longer than a radial trap period. Thus, the atom loss from the center of the cloud during the field inversion process could not be

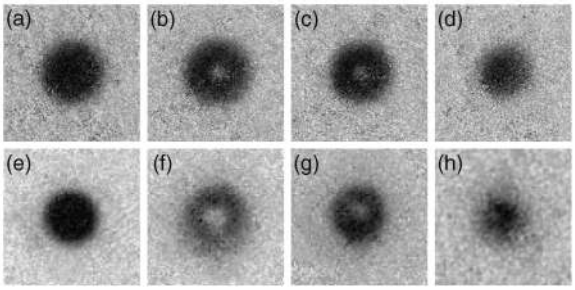

FIG. 2. Observation of vortices formed by imprinting topological phases. Axial absorption images of condensates in the $|1, -1\rangle$ state after 18 ms of ballistic expansion (a) prior to inverting B_z, after inverting B_z, and holding the trapped condensate for (b) 5 ms and (c) 20 ms, and (d) after inverting B_z and then returning it to its original direction. Axial absorption images of condensates in the $|2, +2\rangle$ state after 7 ms of ballistic expansion (e) prior to inverting B_z, after inverting B_z, and holding the trapped condensate for (f) 0 ms and (g) 5 ms, and (h) after inverting B_z and then returning it to its original direction. The field of view is (a)–(d) 570 μm $\times$ 570 μm and (e)–(h) 285 μm $\times$ 285 μm.

responsible for the observed density depletions. Typical $|1, -1\rangle$ ($|2, +2\rangle$) condensates after inverting the axial bias field contained up to 1×10^6 atoms (0.5×10^6 atoms) with a Thomas-Fermi radius $R_{\mathrm{TF}} = 5.4 \pm 0.2$ μm ($R_{\mathrm{TF}} = 4.5 \pm 0.2$ μm) in a trap with radial frequency $\omega_\perp = 2\pi \times 250$ Hz ($\omega_\perp = 2\pi \times 350$ Hz).

The axial angular momentum per particle of the vortex states was measured using surface wave spectroscopy [14–16]. A superposition of counterrotating ($m_\ell = \pm 2$) quadrupolar ($\ell = 2$) surface waves was excited in the condensate by radially displacing the magnetic trap center for 200 μs. Here ℓ and m_ℓ characterize the angular momentum and its projection along the z axis of the quadrupole modes, respectively. This created an elliptical condensate cross section with time-dependent eccentricity. In the absence of a vortex, the $m_\ell = \pm 2$ quadrupole modes are degenerate and the axes of the elliptical condensate cross section remain fixed in time. This degeneracy is lifted by the presence of a vortex, causing the axes to precess in the direction of the fluid flow. The precession rate, $\dot{\Theta}$, is given by [14–16]

$$\dot{\Theta} = \frac{\langle L_z \rangle}{2M\langle r_\perp^2 \rangle}, \tag{8}$$

where $\langle L_z \rangle$ is the axial angular momentum per particle characterizing the vortex state, M is the atomic mass, and $\langle r_\perp^2 \rangle = \langle x^2 + y^2 \rangle$ is the mean-squared trapped condensate radius with vortices present.

By measuring the precession rate of the quadrupole axes and the mean-squared radius of the condensate in the trap, the axial angular momentum per particle was determined. After exciting the quadrupolar modes, the condensate evolved in the trap for variable times in the range 0.2–7.4 ms. The condensate was then released from the trap and imaged with resonant light after ballistic expansion as shown in Figs. 3(a)–3(l). The resulting images were fit to an elliptical Thomas-Fermi profile to determine the orientation of the quadrupole axes. The orientation angle is plotted as a function of time in Fig. 3(m). To determine the mean-squared trapped condensate radius, vortices were imprinted in the condensate but quadrupolar modes were not excited. Images of ballistically expanded condensates similar to those in Figs. 2(b), 2(c), 2(f), and 2(g) were fit to a Thomas-Fermi profile with a circular cross section. The fitting routine ignored the central region of the cloud where the density was depleted due to the vortex core. The mean-squared trapped condensate radius was derived through the relation

$$\langle r_\perp^2 \rangle = \frac{2}{7} \frac{R_\perp^2}{1 + \omega_\perp^2 \tau^2}, \tag{9}$$

where $R_\perp$ is the Thomas-Fermi radius of the condensate after ballistically expanding for a time τ from a trap with radial frequency $\omega_\perp$. The factor $1 + \omega_\perp^2 \tau^2$ accounts for the change in Thomas-Fermi radius during the expansion process [22], and the factor $2/7$ results from averaging over the inhomogeneous condensate density distribution assuming no vortices are present. For low angular momentum vortex states, the density depletion at the vortex core does not significantly modify the density distribution of the condensate, and we expect the $2/7$ factor to still be accurate [23].

For $|1, -1\rangle$ condensates, the quadrupole oscillation was excited after a delay of 0, 5, and 20 ms from the completion of the inversion of the axial bias field. The measured axial angular momenta per particle were $(+1.9 \pm 0.3)\hbar$, $(+2.1 \pm 0.3)\hbar$, and $(+1.9 \pm 0.2)\hbar$, respectively. The uncertainty in the measurement arises from the linear fit to the precession angle and the determination of $\langle r_\perp^2 \rangle$. For $|2, +2\rangle$ condensates, the quadrupole oscillation was excited immediately upon the completion of the inversion of the axial bias field. The measured axial angular momentum per particle was $(-4.4 \pm 0.4)\hbar$. For both internal states, the measurements are consistent with the predicted axial angular momentum per particle of $-2m_F\hbar$ [2–5].

Multiply charged vortices are unstable against decay into singly charged vortices [24]. From our experiments, we cannot determine if the condensate contained one multiply charged vortex or multiple, singly charged vortices. If multiple vortices were present, they must be closely spaced since they were not resolved after ballistic expansion. Furthermore, if the singly charged vortices had moved apart considerably, it would have lowered the extracted value of $\langle L_z \rangle$ [15], which was not observed even with delayed probing.

In conclusion, we have used topological phases to imprint vortices in a Bose-Einstein condensate. Higher angular momentum states can be generated by using higher-order, axisymmetric multipole magnetic fields. In general, this phase-imprinting technique opens the

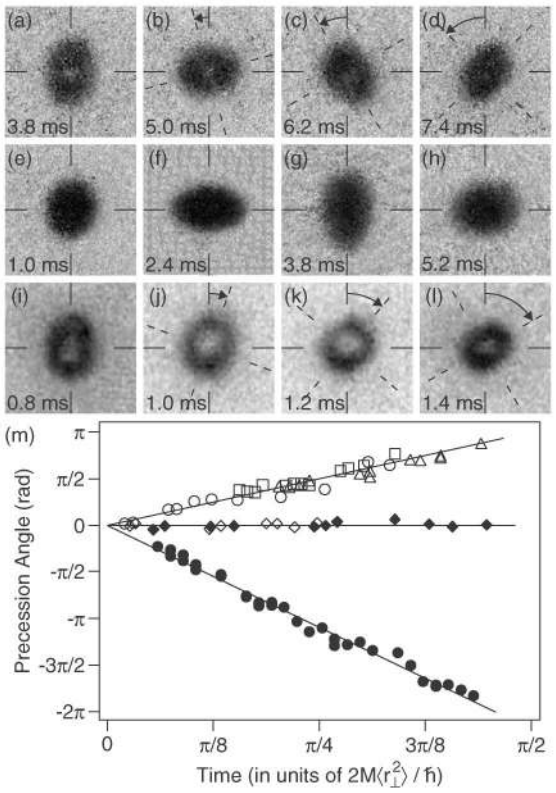

FIG. 3. Surface wave spectroscopy. Axial absorption images after 18 ms of ballistic expansion of $|1, -1\rangle$ condensates undergoing a quadrupole oscillation (a)–(d) in the presence of a vortex and (e)–(h) in the absence of a vortex. Successive images were taken during successive half periods of the quadrupole oscillation such that the short and long axes of the elliptical cross section were exchanged. Images (a)–(d) show counterclockwise (positive) precession of the quadrupole axes, while images (e)–(h) show no precession. (i)–(l) Axial absorption images after 7 ms of ballistic expansion of $|2, +2\rangle$ condensates undergoing a quadrupole oscillation in the presence of a vortex. The images were taken during a single half period of the quadrupole oscillation. Images (i)–(l) show clockwise (negative) precession of the quadrupole axes. The field of view is (a)–(h) $570\ \mu\text{m} \times 570\ \mu\text{m}$ and (i)–(l) $285\ \mu\text{m} \times 285\ \mu\text{m}$. (m) Precession angle vs time in the presence of a vortex for $|1, -1\rangle$ condensates measured after a delay of 0 ms (open circles), 5 ms (open squares), and 20 ms (open triangles) from the completion of the inversion of the axial bias field, in the absence of a vortex for $|1, -1\rangle$ (open diamonds) and $|2, +2\rangle$ (filled diamonds) condensates, and in the presence of a vortex for $|2, +2\rangle$ condensates measured immediately upon the completion of the inversion of the axial bias field (filled circles).

potential for studying the stability of multiply charged vortices and the dynamics of vortex-vortex interactions at short separations.

We thank J. R. Abo-Shaeer for a critical reading of the manuscript. This work was funded by ONR, NSF, ARO, NASA, and the David and Lucile Packard Foundation. A. E. L. acknowledges additional support from NSF.

*5th Physikalisches Institut, University of Stuttgart, 70550 Stuttgart, Germany.
†Electronic address: http://cua.mit.edu/ketterle_group/

[1] M. V. Berry, Proc. R. Soc. London A **392**, 45 (1984).
[2] M. Nakahara, T. Isoshima, K. Machida, S.-i. Ogawa, and T. Ohmi, Physica (Amsterdam) **284-288B**, 17 (2000).
[3] T. Isoshima, M. Nakahara, T. Ohmi, and K. Machida, Phys. Rev. A **61**, 063610 (2000).
[4] S.-I. Ogawa, M. Möttönen, M. Nakahara, T. Ohmi, and H. Shimada, Phys. Rev. A **66**, 013617 (2002).
[5] M. Möttönen, N. Matsumoto, M. Nakahara, and T. Ohmi, cond-mat/0205542.
[6] M. R. Matthews, B. P. Anderson, P. C. Haljan, D. S. Hall, C. E. Wieman, and E. A. Cornell, Phys. Rev. Lett. **83**, 2498 (1999).
[7] K. W. Madison, F. Chevy, W. Wohlleben, and J. Dalibard, Phys. Rev. Lett. **84**, 806 (2000).
[8] J. R. Abo-Shaeer, C. Raman, J. M. Vogels, and W. Ketterle, Science **292**, 476 (2001).
[9] P. C. Haljan, I. Coddington, P. Engels, and E. A. Cornell, Phys. Rev. Lett. **87**, 210403 (2001).
[10] E. Hodby, G. Hechenblaikner, S. A. Hopkins, O. M. Maragò, and C. J. Foot, Phys. Rev. Lett. **88**, 010405 (2002).
[11] S. Inouye, S. Gupta, T. Rosenband, A. P. Chikkatur, A. Görlitz, T. L. Gustavson, A. E. Leanhardt, D. E. Pritchard, and W. Ketterle, Phys. Rev. Lett. **87**, 080402 (2001).
[12] Z. Dutton, M. Budde, C. Slowe, and L. V. Hau, Science **293**, 663 (2001).
[13] B. P. Anderson, P. C. Haljan, C. A. Regal, D. L. Feder, L. A. Collins, C. W. Clark, and E. A. Cornell, Phys. Rev. Lett. **86**, 2926 (2001).
[14] F. Zambelli and S. Stringari, Phys. Rev. Lett. **81**, 1754 (1998).
[15] F. Chevy, K. W. Madison, and J. Dalibard, Phys. Rev. Lett. **85**, 2223 (2000).
[16] P. C. Haljan, B. P. Anderson, I. Coddington, and E. A. Cornell, Phys. Rev. Lett. **86**, 2922 (2001).
[17] Y. V. Gott, M. S. Ioffe, and V. G. Tel'kovskii, Nucl. Fusion Suppl. **3**, 1045 (1962).
[18] D. E. Pritchard, Phys. Rev. Lett. **51**, 1336 (1983).
[19] T. L. Gustavson, A. P. Chikkatur, A. E. Leanhardt, A. Görlitz, S. Gupta, D. E. Pritchard, and W. Ketterle, Phys. Rev. Lett. **88**, 020401 (2002).
[20] A. Görlitz, T. L. Gustavson, A. E. Leanhardt, R. Löw, A. P. Chikkatur, S. Gupta, S. Inouye, D. E. Pritchard, and W. Ketterle, cond-mat/0208385.
[21] A. E. Leanhardt, A. P. Chikkatur, D. Kielpinski, Y. Shin, T. L. Gustavson, W. Ketterle, and D. E. Pritchard, Phys. Rev. Lett. **89**, 040401 (2002).
[22] Y. Castin and R. Dum, Phys. Rev. Lett. **77**, 5315 (1996).
[23] F. Dalfovo, S. Giorgini, L. P. Pitaevskii, and S. Stringari, Rev. Mod. Phys. **71**, 463 (1999).
[24] P. Nozières and D. Pines, *The Theory of Quantum Liquids* (Addison-Wesley Publishing Co., Reading, MA, 1990), Vol. II.